Superdispersion in homogeneous unsaturated porous media using NMR propagators

V. Guillon,[1,2] M. Fleury,[1] D. Bauer,[1] and M. C. Neel[2]
[1]*Université d'Avignon et des Pays de Vaucluse, UMR 1114 EMMAH, 84018, Avignon, France*
[2]*IFP Energies nouvelles, 92852 Rueil-Malmaison, France*
(Received 3 October 2012; revised manuscript received 29 January 2013; published 12 April 2013)

The NMR propagator technique allows the measurements of the variance $\sigma^2 = \langle(\xi - \langle\xi\rangle)^2\rangle$ of the displacements as a function of time t when flowing in a porous media. The time dependence of σ is a very sensitive test of Gaussian behavior compared to the analysis of the shape of the propagators. Superdispersion occurs when $\sigma^2 \propto t^\alpha$ with the exponent α larger than 1. In a homogeneous 30-μm grain pack and $10 < \mathrm{Pe} < 35$, we observed weak superdispersion in saturated conditions ($\alpha = 1.17$) and gradually strong superdispersion as the water saturation decreases (up to $\alpha = 1.5$) during steady-state oil-water two-phase flow. In saturated conditions, the corresponding longitudinal propagators and breakthrough curves are Gaussian or nearly Gaussian, whereas in two-phase conditions, the longitudinal propagators are nonsymmetric and the breakthrough curves show a tail at long times.

DOI: 10.1103/PhysRevE.87.043007 PACS number(s): 47.56.+r

I. INTRODUCTION

Dispersion in porous media mainly originates from three different mechanisms: (i) Taylor dispersion caused by molecular diffusion, allowing particles to move from one streamline to another; (ii) mechanical dispersion due to the numerous restrictions in the porous media; and (iii) stagnant zones where the flow is very slow, resulting in long tails on tracer curves (concentration vs time at the outlet of a core after a step injection). Dispersion in porous media has been studied for a long time using tracer tests analyzing essentially the so-called breakthrough curves, and these studies performed in simple packs led to a general description of the longitudinal dispersion coefficient D expressed as a function of Péclet number (Pe) [1] (available in textbooks such as Ref. [2]). Using such techniques, a large amount of literature is available, mostly in saturated conditions (see Sahimi's book for a literature review [3]). Dispersion is sometimes found to be anomalous, meaning that tracer curves are non-Gaussian. This is the case, for example, in complex carbonates with millimeter-scale heterogeneities; with the help of local concentration measurements, one may find a dispersion coefficient depending on length [4]. Small deviations from Gaussian behavior can also be found in homogeneous grain packs after careful measurements of the breakthrough curves [5]. Alternatively, the NMR propagator technique brings crucial information with the possibility of studying the dependence of dispersion with time and this is the approach taken in this work. Using the time variable, dispersion is non-Gaussian if the variance of the displacements of the tagged molecules does not grow linearly with time, $\sigma^2 \propto t^\alpha$. We can distinguish subdispersion ($\alpha < 1$) and superdispersion ($\alpha > 1$) with an upper limit $\alpha = 2$ characterizing a ballistic regime. In addition, such experiments can be related almost directly to random walk models representing the displacement probability of particles in space and time with Gaussian or non-Gaussian statistics [6,7].

The study of dispersion as a function of time can be misleading because non-Gaussian behaviors can be observed in the preasymptotic regime and in this case it does not mean anomalous dispersion. In the preasymptotic regime, the mean displacement is not large enough compared to the local flow field heterogeneities, and the NMR measurements are sensitive to the local pore geometry. In bead packs (152 and 215 μm), Scheven and Sen [8] proposed two combined criteria for observing Gaussian propagators: (i) when the average displacement is sufficiently large compared to the bead size (criterion $\langle\xi\rangle > 10d_g$), meaning that the mechanical dispersion reached a steady state, and (ii) when the molecular diffusion is large enough to allow particles to probe several streamlines (criterion $L_d = \sqrt{2D_m t} > 0.3d_g$, where D_m is molecular diffusion). If we assume that these criteria determined on bead packs are applicable to other systems, if non-Gaussian propagators are found above these limits, then dispersion will be truly anomalous. In practice, relatively small grain sizes are necessary to reach the two abovementioned criteria because the time scales that can be explored with NMR are limited by the magnetization lifetime, which is itself driven by surface relaxation. A more general approach is to consider the velocity correlation length d_c to establish the length scale characterizing the flow field. Khrapitchev and Callaghan [9] measured the velocity autocorrelation function on a 500-μm latex sphere pack at high Péclet number ($\mathrm{Pe} \approx 1000$) and found that it reaches zero at about $4d_g$, thus smaller than $10d_g$.

In many field applications, dispersion may occur in the presence of two fluids (e.g., oil and water, air and water). However, laboratory experiments on dispersion in unsaturated conditions or two-phase flows using classical tracer experiments are less numerous than those in saturated conditions due to the obvious difficulty of controlling or maintaining a constant saturation while injecting a tracer. In the context of enhanced oil recovery, Delshad *et al.* [10] studied dispersion in the oil and water phases in sand packs and Berea sandstones and found an increase by a factor of 3 of the dispersion coefficients in the water phase as the water saturation decreases. In the work of Bacri *et al.* [11], anomalous breakthrough curves were measured on the nonwetting phase and these authors interpreted their results as a size effect. In the field of hydrology [12–15], experiments are performed in the air-water fluid system with saturation depending on flow rates,

yielding a large variation of Péclet numbers between different experiments. Hence, dispersion coefficients do not increase monotonically as a function of saturation [15]. However, when appropriately scaled, dispersivity increases by a factor of 3 and up to a factor of 10 [13] at low Péclet number. From the NMR point of view, Rassi *et al.* [16] performed propagator measurements on 100-μm glass beads in air-water unsaturated conditions but dispersion coefficients were not analyzed. In a pioneering work, De Gennes [17] proposed a theoretical framework for dispersion in unsaturated conditions based on percolation theory and considering stagnation effects. However, this is mostly applicable to the nonwetting phase, whereas our work concerns the wetting phase.

We focus in this work on the superdispersion of the flow in granular porous media in the asymptotic and quasiasymptotic regime for saturated and unsaturated conditions, respectively. Using granular packs as model porous system has several advantages; they are more representative of natural porous media with nonsmooth surfaces as opposed to bead packs, they have a single characteristic length scale d_g given by the grain size, and the pore space is very "open" such that stagnant zones due to the pore structure are very limited. We first present the porous media used and the experimental setups, the NMR sequences, and processing. In the second part we present the results for saturated conditions to be used as a reference, and then the results for unsaturated conditions using the oil-water fluid system. To link the traditional tracer approach to NMR propagators, we also performed such tracer experiments in the same experimental setup.

II. EXPERIMENT

In this section, we describe the two NMR instruments and the velocimetry sequences used, the porous media, the techniques for varying and measuring saturation, and the deuterium tracer tests.

A. Grain packs and experimental setup

We prepared different grain packs made of SiC grains (P. Wolters, Germany) having a narrow size distribution (8, 18, 30, 50, 80, and 110 μm) as determined by diffraction techniques. Such material is convenient to produce model granular porous media and has been used in the past for other NMR studies [18]. The grains have sharp edges with a morphology characteristic of crushed material and close to natural sands, although natural grains are in general more rounded due to their geological history [19]. The raw material, however, must be cleaned with acid to remove fines and paramagnetic impurities that would otherwise generate lower NMR relaxation times. Two cells of different lengths were used in two NMR devices (Fig. 1) presented below. In the short cells (length 50 mm, inner diameter 30 mm), the porosities of the different packs are respectively 49.4%, 42.9%, 40.1%, 40.4%, 38.8%, and 37.7% for the 8-, 18-, 30-, 50-, 80-, and 110-μm grain sizes, respectively (it is more difficult to pack the smallest grain size due to increasing surface forces). In the long cell (length 300 mm, inner diameter 26 mm), the average porosity of the 30-μm grain pack is 42%. The NMR porosity profile (described later in Sec. II B) is fairly uniform (Fig. 2) and the measured permeability is 296 mD.

Two NMR instruments (2 and 20 MHz) equipped with two different cells were used (Fig. 1). The cells of the 2-MHz/50-mm probe instrument (Oxford Instruments) are composed of glass tubes of inner diameter 30 mm with Teflon end caps allowing fluid circulation. The length of the packs is 60 mm and corresponds to the length of the NMR antenna (solenoid). In this classical design used in many published works, the displacement of water molecules is detected in the entire cell and, thus, we include the possible imperfections of the flow induced by the presence of the inlet (outlet) at the beginning (end) of the porous medium. It cannot be used for unsaturated conditions and the relatively low signal-to-noise ratio due to the low frequency would require long experiments at low water saturation.

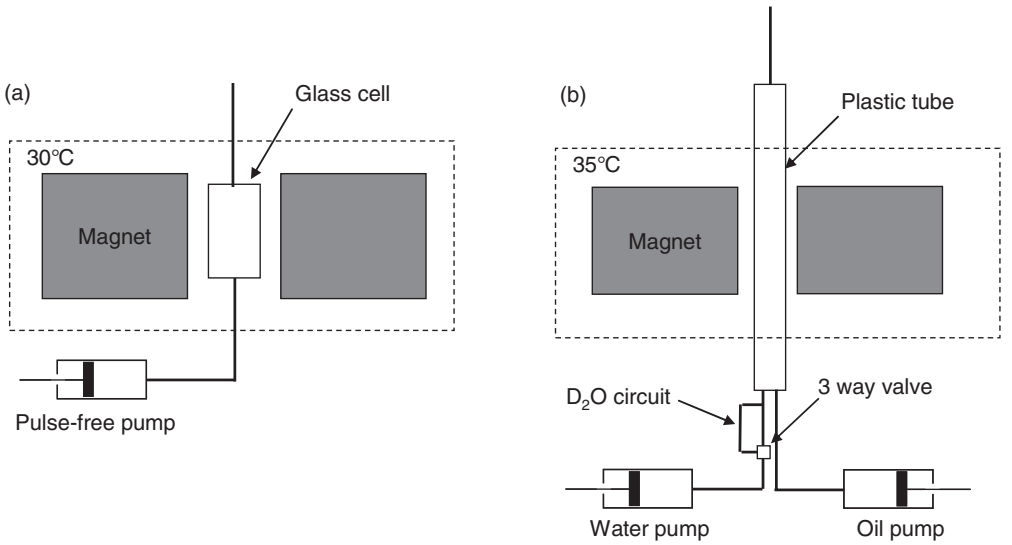

FIG. 1. Experimental setups. (a) For the 2-MHz, 50-mm system, the grain pack has a length of 60 mm, similar to the antenna. (b) For the 20-MHz, 30-mm imaging system, the grain pack has a length of 27 cm. The three-way valve allows the flow to be diverted in a parallel circuit full of deuterium for tracer measurements.

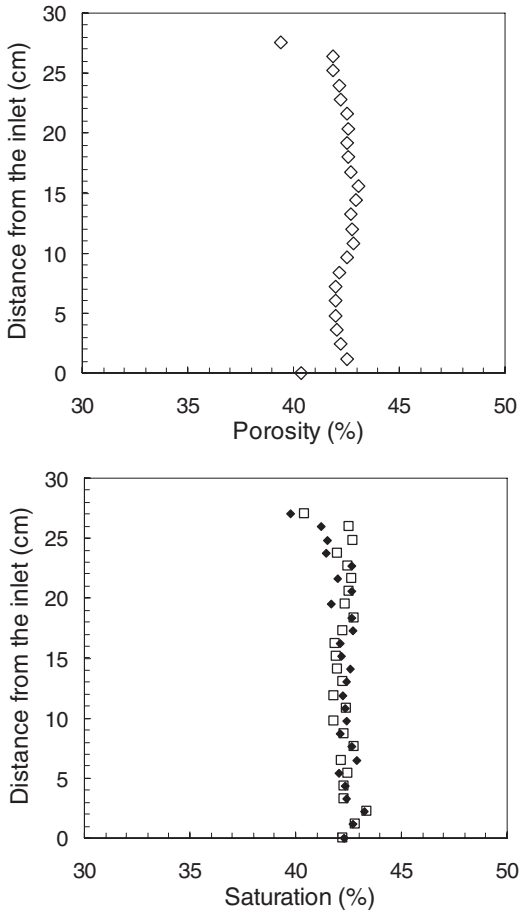

FIG. 2. Porosity and saturation profiles measured by NMR every centimeter for the 30-μm grain pack column. Each point corresponds to the average porosity in a slice of thickness 8 mm. In the saturation graph, two experiments with the same flow rates are shown, resulting in similar profiles. In the porosity profile, the two end points are influenced by the end pieces of the cell.

For the NMR imaging system (Oxford Instruments, 20-MHz, 30-mm probe), the cell is a long plastic (Macrolon) tube of length 300 mm and inner diameter 26 mm. In this situation where the cell is much larger than the NMR antenna, we used a slice selection technique of thickness 8 mm (see next paragraph) and performed all measurements within this slice (velocity, porosity, saturation). The end caps at both ends of the tube have two entries for us to be able to inject two fluids simultaneously for the study of unsaturated conditions. At the contact with the grains, the fluid injection is optimized by using a spiral. The NMR instrument is open at the bottom, and so the cell can be moved up and down to locate the NMR measurement slice closer to or farther from the inlet or outlet. This was especially useful to evaluate porosity and saturation in the entire column.

To vary the water saturation of the pack, a standard steady-state co-injection technique [20] was applied using water and a fluorinated oil (FC77 from 3M company, viscosity 1.4 cP at 25 °C, oil-water interfacial tension 43 mN/m). Hence, only the water phase is examined. Air injection has also been tested but, due to its compressibility and very unfavorable mobility compared to water, stable and low enough saturation could not be reached. The saturation can be tuned almost as desired by adjusting the flow rate of each fluid relative to the other. Since we follow only the wetting phase, we usually set the desired water flow rate for NMR measurements and adjust the oil flow rate increasingly to decrease the saturation. All measurements presented here were performed in a drainage mode (decreasing water saturation) and, when we repeated measurements, the starting saturation was always set back at 100% water. Pulse-free pumps (Quizix QX6000) were used to avoid disturbances of the measured propagator due to rapid flow rate fluctuations.

The NMR technique was also used to perform a standard tracer test measurement. In such experiments, one usually injects a miscible fluid of same density and viscosity whose concentration can be detected by any appropriate technique (electrical, acoustic, UV spectroscopy, computed tomography scan), locally or at the outlet of the cell. In our case, we used deuterium as a tracer, and to adjust the density and avoid gravity effects the grain pack was saturated with a NaCl brine of salinity 150 g/l. In practice, without stopping the brine flow rate, a set of valves located as close as possible to the cell inlet allows the brine flow to be diverted into a parallel circuit full of deuterium (Fig. 1). The volume of deuterium tracer (5 cm^3, about 10% of the pore volume) was adjusted using an appropriate length of tubing in this parallel circuit. This simple system allows us to inject a step deuterium tracer, which is later detected in the selected slice. The deuterium concentration C in the slice is linked to the measured total magnetization M in the slice (described later) according to

$$C(t) = 1 - \frac{M(t) - M_R}{M_R}, \quad t \to \frac{V(t)}{V_p}, \tag{1}$$

where M_R is a reference (baseline) magnetization measured before injection and checked at the end of the tracer test. A change of variable, moreover, converts time into the ratio of injected volume $V(t)$ per pore volume V_p, defined as the pore volume from the inlet up to the center of the measurement slice. In this representation, C achieves its maximum at $V/V_p = 1$ in the case of Gaussian dispersion. We call $C(t)$ local breakthrough curves by analogy with standard experiments, although they are not measured at the outlet of the cell.

We varied the flow rates from 50 up to 2000 ml/h, and the NMR observation time from 20 up to 1000 ms depending on relaxation time. Relaxation time decreases linearly with decreasing saturation, thus reducing the possibility of observing long dispersion times. In saturated and unsaturated conditions, the Péclet number is calculated with the grain size d_g and the average velocity of the flow, $\langle v \rangle$:

$$\mathrm{Pe} = \frac{\langle v \rangle d_g}{D_m}. \tag{2}$$

B. NMR sequences and data processing

The sequences used to measure displacement distributions are shown in Fig. 3. Both sequences are alternate pulsed field gradient stimulated echo sequences but the one used in the imaging system has the additional capability of a slice selection as well as the possibility of measuring both longitudinal and

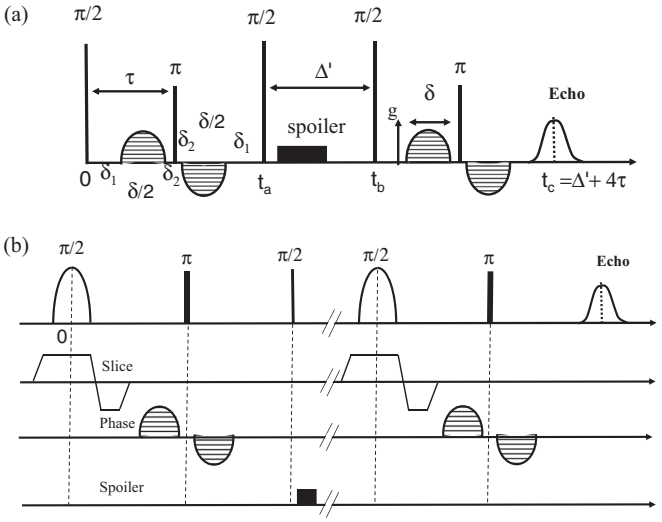

FIG. 3. NMR sequences for measuring propagators: (a) the sequence used in the 2-MHz system with only vertical gradient directions and (b) the sequence used in the 20-MHz imaging system in which a slice selection is performed. The phase encoding gradient direction can be set in three perpendicular directions. The same time delays apply to this sequence using the center of pulses.

transverse displacements. In both sequences, for the coding and decoding of spin positions, the gradient pulses are centered around the π pulse in order to better compensate for eddy currents ($\delta_2 = 100\ \mu$s) and limit the effect of uncontrolled gradients (internal or residual). To build the NMR signal $E(q,t)$, echo amplitudes are collected for different values of wave number q and observation time t according to

$$t = \Delta' + 2\tau - \frac{1}{3}\delta - \delta_2, \quad q = \frac{\gamma g_{\max}\delta}{2}, \tag{3}$$

where $g_{\max}$ is the maximum amplitude of the gradient pulse, and γ the proton giromagnetic ratio ($\gamma/2\pi = 42.58$ MHz/T). The factor of 2 in the q calculation originates from the gradient shape. The signal $E(q,t)$ is acquired at a fixed time and for a range of q values such that it reaches the noise level at large q (q is varied using different gradient values $g_{\max}$, up to about 150 G/cm). For simplicity, we indicate the uncorrected observation time $\Delta' + 2\tau$ in the results or graphs but the above time t was used to process data. Typically, we used $\tau = 1.25$ ms, $\delta = 1.5$ ms, and $\delta_2 = 0.2$ ms in the 2-MHz system, and $\tau = 3$ ms, $\delta = 4$ ms, and $\delta_2 = 0.1$ ms in the 20-MHz system. The gradient amplitudes were calibrated by measuring water diffusivity at a controlled and stable temperature in each system. For the slice selection in the imaging system, the soft pulse is a five-lobe sinc function of duration 0.5 ms. The duration of the soft pulse and the slice gradient amplitude are such that the thickness of the slice is 8 mm at midheight. Although smaller values could be set, such thickness was chosen in order to avoid underestimation of velocity due to spins entering or leaving the slice without being labeled or counted.

To determine porosity and saturation in the slice, the total magnetization was measured from the maximum of the free induction decay immediately after the first $\pi/2$ pulse and slice gradient (Fig. 3). Porosity and water saturation in the slice were then calculated from

$$\Phi = \frac{M_{100}}{M_R}, \quad S_w = \frac{M_S}{M_{100}}, \tag{4}$$

where M_R is a reference magnetization measured with the tube full of water, M_{100} is the magnetization at 100% water saturation, and M_S is the magnetization for a given saturation S_w. In fact, this simple principle does not always give precise results because the tuning of the probe is modified by the grains. Hence, the porosity has to be corrected by 3%, a value established using various phantoms. However, the saturation estimations have no correction because the probe tuning does not change (the amount of grains does not change).

The first two cumulants, average displacement $\langle\xi\rangle$ and longitudinal or transverse variance $\sigma^2 = \langle(\xi - \langle\xi\rangle)^2\rangle$, were calculated using the small q expansion:

$$\theta(q,t) = \langle\xi\rangle q, \quad \ln|E(q,t)| = -\tfrac{1}{2}\sigma^2 q^2, \tag{5}$$

where θ is the phase of the complex signal $E(q,t)$ at a fixed observation time t. The two cumulants are obtained by fitting the data up to $q_{\max}$, the upper limit at which the linearity with q or q^2 is lost due to high order terms (Fig. 4). The distributions of displacements (longitudinal or transverse propagators) during

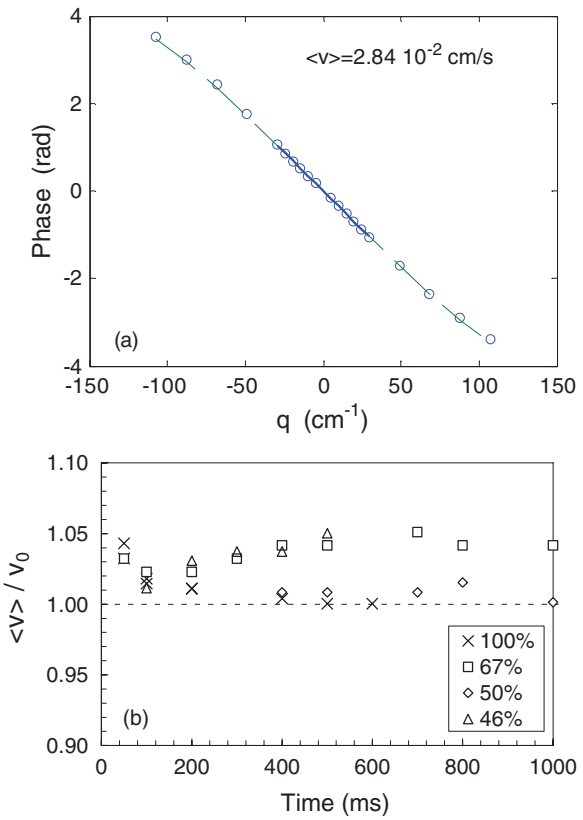

FIG. 4. (Color online) Example of phase data used to calculate (a) the average velocity and (b) the average velocity normalized by the pore velocity v_0 for different observation times and saturation. Long column, 20-MHz imaging system, 30-μm grain pack. The dashed line in (a) indicates a fit with the cumulant of order 3, Pe = 3.2; (b) 1.5 < Pe < 2.3.

the time interval t,

$$P(\xi,t) = \int_{-\infty}^{+\infty} E(q,t)e^{i2\pi q\xi}dq, \tag{6}$$

were calculated using a discrete Fourier transform of the entire signal $E(q,t)$ acquired down to the noise level and using about $50q$ steps. The signal was sampled more densely at small q to provide better estimations of cumulants [hence, we do not use a fast Fourier transform algorithm to calculate propagators]. In our granular pack and experimental system, we do not have problems related to a distribution of relaxation time that occur in natural rocks [21], or excessive internal gradients that could occur at higher field [22]. Indeed, when calculating the average velocity $\langle v\rangle$ at different times, at a fixed flow rate normalized by the pore velocity v_0 calculated with the imposed flow rate, we obtain rather constant values (Fig. 4); at 100% saturation $\langle v\rangle$ is overestimated by 5% at $t = 50$ ms, and this discrepancy decreases for longer times. This has been also observed in bead packs [21], and it cannot be due to random noise or to bad gradient calibration. The detailed explanation of this small systematic deviation is unclear. However, for the same range of q values, one should note that the range of gradient used is larger at short times to produce the same signal attenuation, thus potentially perturbing the measurements. In unsaturated conditions, we have small fluctuations of a few percent but the abovementioned systematic decrease is not observed.

III. RESULTS

We first show the results for saturated media to check as accurately as possible the normal behavior, if it ever does exist. In a prestudy performed in the 2-MHz, 50-mm NMR apparatus, we measured the longitudinal propagator in a series of grain packs with different grain sizes and at a unique flow rate to observe the transition from preasymptotic to the asymptotic regime as a function of grain size. Based on these results, we choose to study in more detail a 30-μm grain pack in a long column using the 20-MHz imaging system as a compromise (a smaller grain size allows the asymptotic regime to be reached more easily, but it produces higher pressure drops as well as shorter relaxation times, reducing the range of possible observation times). In this pack, we establish accurately the time dependence of the variance in saturated and unsaturated conditions.

A. Saturated media

The effect of the grain size on the longitudinal propagators is illustrated in Fig. 5 for the smallest and largest grains. Both measurements were performed at the same imposed flow rate (500 ml/h) yielding similar pore velocity (0.026 and 0.020 cm/s for the 8- and 110-μm grain pack, respectively, Pe = 0.7 and 12.4). Whatever the observation time (from 20 up to 500 ms), the propagators obtained on the smallest grain size are Gaussian within experimental uncertainties (asymptotic regime) and fully non-Gaussian for the largest one, with a tail toward large displacements. For the 110-μm pack, the mean displacement relative to the grain size is not large enough ($\langle\xi\rangle/d_g < 3$ for all times), so the measured displacements are representative of the local geometry with some influence of

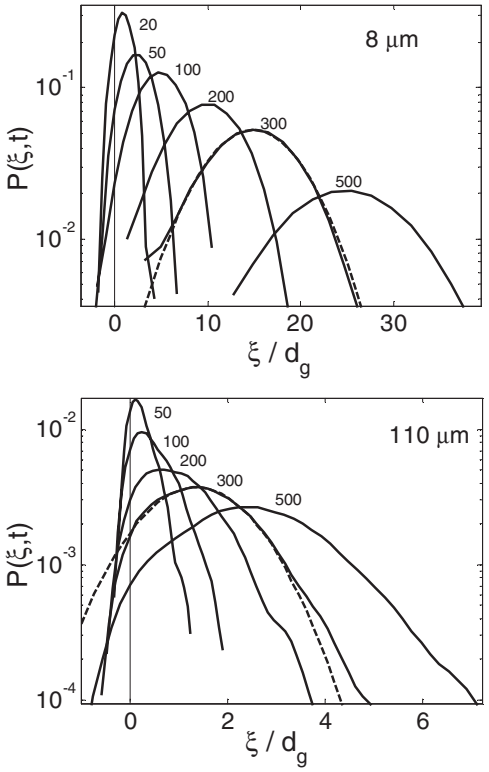

FIG. 5. Longitudinal propagators measured at different observation times (units of milliseconds) on two grain packs made with the smallest (8 μm, Pe = 0.7) and largest grain sizes (110 μm, Pe = 12.4). Short column, 2-MHz system. The dashed line for 300 ms indicates a Gaussian distribution for comparison. For the 110-μm grain pack, the propagators are non-Gaussian.

molecular diffusion and mechanical mixing, which explains why we still see negative displacements even at the largest time. On the contrary, for the 8-μm grain size the propagators are always Gaussian for two reasons: when $\langle\xi\rangle/d_g > 10$ ($t >$ 200 ms), the mechanical mixing is large enough that the local geometry has no effect; when $\langle\xi\rangle/d_g < 10$ ($t <$ 200 ms), the molecular diffusion is large enough that the local geometry is smeared out. Indeed, the diffusion length relative to the grain size is large, $L_d/d_g > 1.3$, and much larger than the criterion of 0.3 proposed by Scheven and Sen [8]. When the grain size increases, propagators become gradually nonsymmetric and the asymptotic regime, which is our main interest, is gradually more difficult to reach. It can be noted that we never observed bimodal propagators with a distinct peak close to zero displacement at short time or for large grain sizes (e.g., 110 μm). From the literature and considering sphere packs only, such a feature is not systematically observed. Strong and distinct peaks are observed by some authors [16,23] but are absent or very weak in some other works [8,21,24] and the required conditions for observing such strong bimodal propagators remain unclear.

Following this preliminary work, we choose to study in more detail the 30-μm grain pack in the long column. For this grain size, the relaxation time is not too short ($T_2 = 294$ ms) and allows long enough dispersion times to be studied, and the permeability is not too small (296 mD), allowing large enough flow rates to be used because the pressure

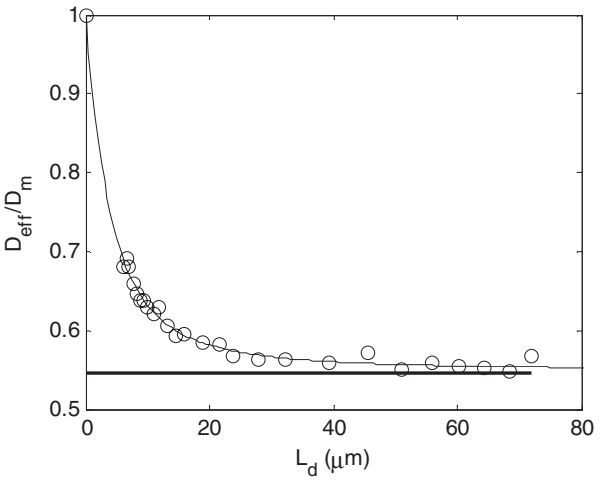

FIG. 6. Effective diffusion vs time curve in the absence of flow for the 30-μm grain pack (2-MHz system). The horizontal line represents the asymptotic value obtained from electrical measurements performed independently. The data points are represented by circles whose diameter corresponds to the vertical error bar.

drop that can be sustained by the plastic cell is limited to 15 bar. In addition, the diffusion criterion is achieved for all experimental times ($L_d/d_g > 0.34$ for $t > 20$ ms) and, thus, we expect to be mostly in the asymptotic regime. On the 30-μm grain and in the absence of flow, we also measured the time-dependent diffusion curve (Fig. 6, performed in the 2-MHz device using a range of observation times t from 8 up to 1000 ms). As expected, the effective diffusion D_{eff} calculated from the second moment and normalized by the molecular diffusion D_m decreases gradually to reach the limit given by the electrical tortuosity measured independently. Strictly speaking, this implies a subdiffusive regime ($\sigma^2 \propto t^\alpha$ with $\alpha < 1$). However, the strongest variation of D is occurring below a diffusion length of about 10 μm ($t = 20$ ms) and, hence, it has a minor effect on the time dependence when considering the range $t > 20$ ms; thus, we cannot observe subdispersion at small Pe as will be seen later. The measured curve also allows us to determine the solid specific surface compared to bead packs: from the initial slope of the $D(t)$ curve, we calculated the volume-to-surface ratio of this medium according to Ref. [25] and obtained $V/S = 1.72$ μm, a value about half as large as that in a bead pack made with spheres of the same diameter (30 μm) and same porosity (i.e., the specific surface is twice as large).

On the 30-μm grain pack in the long column, we measured the longitudinal and transverse propagators for a large variety of flow rates (50–2000 ml/h) and time (20–1000 ms). The measurement slice is located 8 cm from the inlet (see Fig. 2). The propagators were found to be nearly Gaussian and σ^2 increases with the flow rate, as expected due to the general dependence of dispersion with the Péclet number. For longitudinal displacement, we expected to have $\sigma^2 \propto t^\alpha$ with α close to 1 for every flow rate (α is calculated separately for each flow rate). Instead we observed an increase of α with the flow rate or the velocities (Fig. 7). At the highest velocities or Pe, α tends to stabilize around a value of 1.17, a slope observed in the range $\langle\xi\rangle/d_g > 7$ for which the mechanical mixing is stabilized. At the lowest velocities or Pe, dispersion is dominated by diffusion and we do not deviate from normal

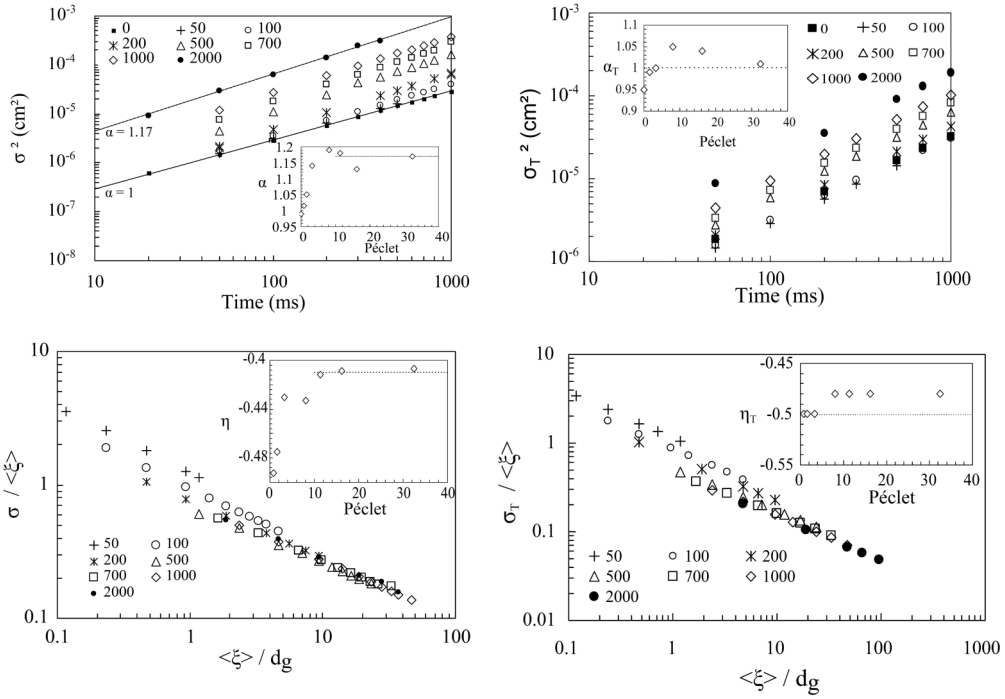

FIG. 7. Longitudinal (σ^2) and transverse (σ_t^2) variance for all experimental conditions, long-column, 20-MHz system, 30-μm grain size, slice position at 8 cm from inlet. Top: variance vs time. Bottom: same data but normalized. The insets indicate the slope α or η of the power laws. The numbers indicate the flow rates in ml/h. The Péclet number is 0, 0.8, 1.6, 3.2, 8.1, 11.3, 16.2, and 32.4 for 0, 50, 100, 200, 500, 700, 1000, and 2000 ml/h, respectively.

behavior ($\alpha = 1$). For the highest velocities, α values larger than 1 imply that the propagator is not strictly Gaussian and this is indeed the case after careful examination, but the time dependence is a much more sensitive and convincing evidence than the analysis of propagators that are always perturbed by Fourier transform processing. The exponents α are determined from the fit of the variance vs time and we estimate that the largest error interval on the exponent α is ± 0.04 (and consequently ± 0.02 on η; see next paragraph). For transverse displacements, σ_t is found to follow normal behavior with α taking values around 1 (the mean value is 1.01 with error bars on the data points of ± 0.04; see Fig. 7), and the corresponding transverse propagators are Gaussian (not shown). The dispersion coefficients calculated from these variance measurements are presented later, together with the results obtained in unsaturated conditions, and compared with literature data.

Another equivalent representation of the data is to search for a power law $\sigma / \langle \xi \rangle \propto (\langle \xi \rangle / d_g)^{\eta}$ (with $\eta = \alpha/2 - 1$) as in Ref. [26]. In this representation, the variable $\langle \xi \rangle / d_g$ is a combination of time and flow rate (Fig. 7) and all data tend to form a unique curve when $\langle \xi \rangle / d_g > 7$, close to the proposed criterion of 10. This collapse is explained by the fact that the asymptotic regime is reached. It suggests a criterion that can be applied to any porous system without the knowledge of the grain or pore size. Below that limit, however, we see a clear separation of the data points (and not a change of slope) that is not observed in other systems [26]. For our data set, the highest value of η is -0.41. For comparison, on 100-μm bead packs in the preasymptotic regime, it was found to be $\eta = -0.46$, closer to -0.5 [26]. On consolidated heterogeneous rocks for which a stagnant peak is observed, η tends to deviate further (for a Bentheimer sandstone, $\eta = -0.36$, and for a Portland carbonate, $\eta = -0.24$, [26]). On breakthrough curves performed on a sand pack, very careful experiments and analysis also allow us to detect very small deviations from the normal behavior in homogeneous systems [5].

B. Unsaturated media

The weak superdispersion observed in saturated conditions is severely amplified in unsaturated conditions. In a similar way, we measured longitudinal and transverse propagators and cumulants in the wetting phase (water) and varied the saturation using the co-injection technique described in the experimental section (30-μm grain size, long column). In these experiments, we kept the average velocity nearly constant: $1.5 < \mathrm{Pe} < 2.5$. We compare the results with the experiment performed at $S_w = 1$ and at a similar Pe (flow rate of 100 ml/h). This experiment is in the preasymptotic regime and has a nearly normal behavior ($\eta = -0.47$, $\alpha = 1.06$). For longitudinal displacements, we represent the time dependence using the plot of $\sigma / \langle \xi \rangle$ vs $\langle \xi \rangle / d_g$ as for saturated conditions (Fig. 8). The time dependence deviates now severely from the normal behavior: the exponent η increases with decreasing saturation from -0.48 up to -0.25 ($\alpha = 1.5$) at the lowest saturation

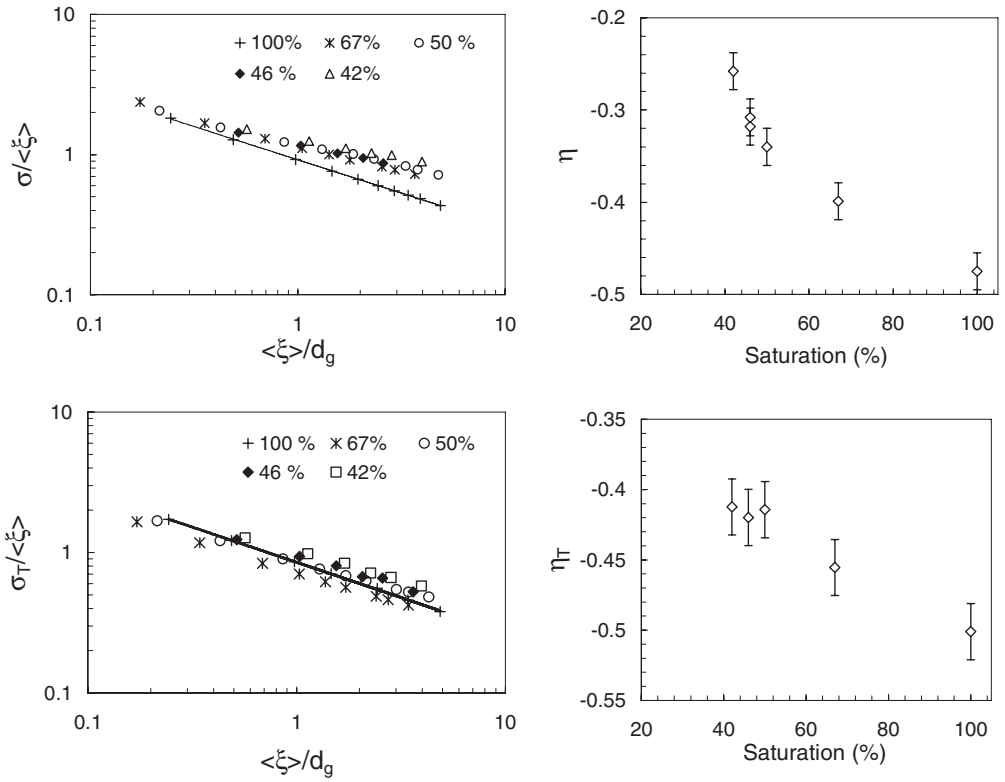

FIG. 8. Evolution of the normalized longitudinal (σ) and transverse (σ_t) square root of variance vs time expressed as the average displacement $\langle \xi \rangle / d_g$ for different saturations. Long-column, 30-μm grain size, slice position at 8 cm from inlet. The Péclet number is 1.6, 1.1, 1.5, 1.6, and 1.8 for $S_w = 100\%$, 67%, 50%, 46%, and 42%, respectively. The line indicates the fit for saturated conditions. The exponents η and η_T of the power laws depend on saturation.

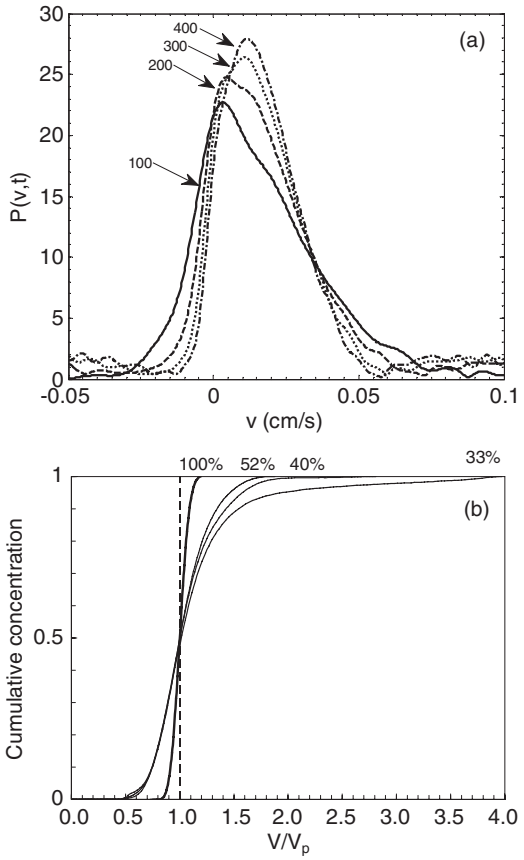

FIG. 9. (a) Longitudinal propagator at different times at $S_w = 46\%$ and (b) tracer experiments performed with deuterium at the position 8 cm from the inlet for different saturations. For the tracer experiment, $\langle v \rangle = 0.014$–$0.021$ cm/s (Pe = 2.1–3.1, $S_w = 100\%$ to 33%) and for the propagators, $\langle v \rangle = 0.015$ cm/s (Pe = 1.6, $S_w = 46\%$).

of 0.42 (the exponent η is calculated by taking all data points such as $\langle \xi \rangle / d_g > 0.5$ and we estimate an error of ± 0.02). Concomitantly, longitudinal propagator asymmetry for the same observation time increases with decreasing saturation, indicating a more heterogeneous flow field (see an example of asymmetry in Fig. 9). Due to pressure limitations in our system, we could not sufficiently increase the flow rate in order to reach larger values of the ratio $\langle \xi \rangle / d_g$. Despite this limitation, the saturation has an important effect on dispersion, not only on the absolute values but also on the time dependence. Remarkably, for transverse displacements, σ_t is also affected by saturation but to a smaller extent. The exponent η_T varies from normal behavior ($\eta = -0.5$) up to -0.41 (Fig. 8).

Another important experimental evidence of such superdispersion is the tracer experiment that was performed at the same location, 8 cm from the inlet (see Fig. 9; we plotted the cumulative curves for clarity). Deuterium concentration curves vs normalized time V/V_p (Fig. 9) are increasingly nonsymmetric as the water saturation decreases (S_w values are not the same compared to propagator measurements because these experiments were realized separately using high salinity brine). They are clearly qualitatively similar to breakthrough curves observed on unsaturated sands [13,14], with a tail at long times. Since the porosity and saturation profiles are uniform (Fig. 2), we are confident that these anomalous curves are not due to porosity or saturation fluctuations. We are also far enough from the injection inlet that the well known inlet boundary condition can be neglected [2]. For comparison, at a similar velocity and $S_w = 46\%$, longitudinal propagators are also strongly nonsymmetric with a tail extending at large velocity at short time, gradually shifting to a more symmetric one at long time (propagators obtained at 100% saturation at a similar velocity are Gaussian at all times). Clearly, the tail at long time seen in the tracer experiment cannot be associated with stagnant zones as propagators do not show a distinct stagnant peak at any time.

The issue of the asymptotic regime already mentioned above is important because, strictly speaking, breakthrough curves and propagators should be compared only in the asymptotic regime. Since the tracer curves also show a strong non-Gaussian behavior, we are confident that the observed time dependence is not solely due to the preasymptotic regime. One may also question the applicability of the criteria ruling the asymptotic regime to unsaturated conditions ($L_d > 0.3 d_g$, $\langle \xi \rangle > 7 d_g$). For the diffusion criterion, i.e., the possibility for molecules to move to a different streamline in the flow, the grain size scale d_g is rather overestimated since the water phase does not fill the entire pore volume. Hence, if we assume that the nonwetting phase is uniformly distributed in all pores, a more appropriate scale would be the product $d_g S_w$, yielding a more favorable criterion for Gaussian dispersion. From this point of view, diffusion should dominate the system but this is not the case. For the mean displacement criterion, the grain size scale may also not be appropriate, and a length scale defined via the velocity autocorrelation function already mentioned is probably the best. However, it must be measured at high Péclet number and requires appropriate equipment in terms of pressure in the case of small grain sizes. Despite these uncertainties for defining the asymptotic regime in unsaturated conditions, the exponents η or α may deviate further from the observed values if the Pe is increased, by analogy with the saturated conditions for which a stable deviation is reached for a sufficiently large Pe.

The distribution of the fluids in the porous system is also of great importance. Flow visualizations in two-dimensional etched water-wet networks [27–29] show that the wetting phase (water) stays continuous whatever the nonwetting fluid (air or oil). For the nonwetting fluid with an unfavorable mobility ratio (e.g., water-to-air viscosity much smaller than 1), the flow consists of ganglions extending several pore sizes that may break and coalesce constantly. For a nonwetting fluid of viscosity similar to that of water, the nonwetting phase may stay continuous, especially at low water saturation, and such continuity may even be more probable in three dimensions. In our case, we perform the experiments only during drainage, the mobility contrast is favorable, and, therefore, a stable flow is expected, presumably with both continuous wetting and nonwetting phases.

An important consequence of our findings is that the effective dispersion coefficient D_{eff},

$$D_{\text{eff}} = \frac{1}{2} \frac{d\sigma^2}{dt}, \tag{7}$$

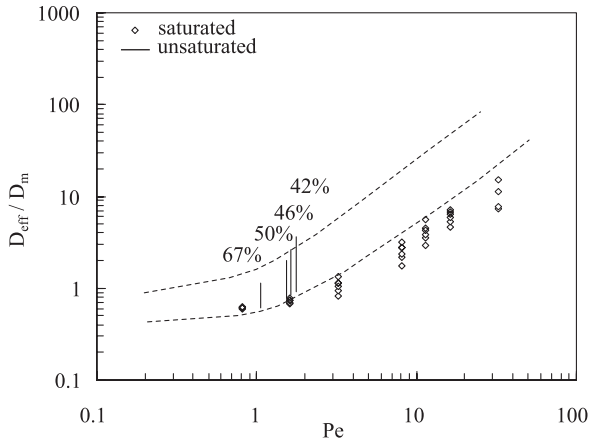

FIG. 10. Normalized effective dispersion coefficients D_{eff} as a function of saturation and Péclet number. Since D_{eff} depends on time, the vertical line (unsaturated) and symbols (saturated) indicate the lower and upper values, respectively, calculated in the experimental time interval. Dotted lines are obtained from a compilation of tracer data found in Ref. [30].

depends on observation time and that this dependence and the value of D_{eff} increase with decreasing saturation. We plot in Fig. 10 the measured effective longitudinal dispersion coefficients with their evolution in the experimental time interval. For saturated conditions and small observation times D_{eff} are slightly lower than values obtained by classical tracer experiments compiled in Ref. [30] and become closer to the tracer values at longer observation times.

IV. CONCLUSION

We measured NMR longitudinal and transverse propagators and local breakthrough curves in a homogeneous 30-μm grain pack column, in saturated and unsaturated conditions. The saturation was varied using a steady-state oil-water two-phase flow technique. In saturated conditions, we observed the transition from the preasymptotic to the asymptotic regime suggested by a stabilization of the exponent α in the time dependence t^{α} of the variance σ^2, or equivalently of the exponent η in the relationship $\sigma/\langle\xi\rangle \propto (\langle\xi\rangle/d_g)^{\eta}$. In this representation, the collapse of data collected at different flow rates and observation times is an alternate way of showing that the asymptotic regime is reached, particularly useful in the case of consolidated natural samples for which the grain size is not necessarily related to the pore size.

In the asymptotic regime, α reaches a value of about 1.17 (or $\eta = -0.41$), whereas longitudinal propagators and local breakthrough curves are Gaussian or nearly Gaussian, but the non-Gaussian nature is ambiguous and depends on noise. The time dependence of the second moment is a robust and convincing way to show weak anomalous behavior, whereas longitudinal propagator measurements and breakthrough curves are much less sensitive to such small deviation. In unsaturated conditions and for different saturation levels (from 67% down to 42%), we observed strong deviations of the above exponents as a function of saturation (up to $\alpha = 1.5$ or $\eta = -0.25$ at $S_w = 0.42$). The corresponding propagators are generally strongly nonsymmetric at short time, and the local breakthrough curves have a tail at large time. Although the criteria for defining the transition to the asymptotic regime should be redefined in unsaturated conditions, the observed strong deviations may still be in the preasymptotic regime and the measured exponents should be considered underestimated. For transverse displacements, normal behavior ($\alpha = 1$) is observed in saturated conditions, and a weaker deviation (up to $\alpha = 1.18$) in unsaturated conditions. Since a distinct stagnant peak is not observed, this anomalous dispersion is not due to stagnant zones in the porous media but to the specificity of the flow field in two-phase flow conditions.

ACKNOWLEDGMENT

The authors have been supported by Agence Nationale de la Recherche (ANR Project No. ANR-09-SYSC-015).

[1] H. O. Pfannkuch, Rev. Inst. Pet. **18**, 215 (1963).
[2] F. A. L. Dullien, *Porous Media, Fluid Transport and Pore Structure* (Academic Press, San Diego, 1992).
[3] M. Sahimi, *Flow and Transport in Porous Media and Fractured Rock* (Wiley-VCH, Weinheim, 2011).
[4] M. Fourar and G. Radilla, Transp. Porous Media **80**, 561 (2009).
[5] M. Levy and B. Berkowitz, J. Contam. Hydrol. **64**, 203 (2003).
[6] R. Metzler and J. Klafter, Phys. Rep. **339**, 1 (2000).
[7] M.-C. Néel, S. H. Rakotonasy, D. Bauer, M. Joelson, and M. Fleury, J. Stat. Mech.: Theory Exp. (2011) P02006.
[8] U. M. Scheven and P. N. Sen, Phys. Rev. Lett. **89**, 254501 (2002).
[9] A. A. Khrapitchev and P. T. Callaghan, Phys. Fluids **15**, 2649 (2003).
[10] M. Delshad, D. J. MacAllister, G. A. Pope, and B. A. Rouse, Soc. Pet. Eng. J. **25**, 524 (1985).
[11] J. Bacri, N. Rakotomalala, and D. Salin, Phys. Fluids A: Fluid Dyn. **2**, 674 (1990).
[12] D. Haga, Y. Niibori, and T. Chida, Water Resour. Res. **35**, 1065 (1999).
[13] N. Toride, M. Inoue, and F. J. Leij, Soil Sci. Soc. Am. J. **67**, 703 (2003).
[14] M. Bromly and C. Hinz, Water Resour. Res. **40**, 5 (2004).
[15] T. Bunsri, M. Sivakumar, and D. Hagare, J. Appl. Fluid Mech. **1**, 37 (2008).
[16] E. M. Rassi, S. L. Codd, and J. D. Seymour, New J. Phys. **13**, 015007 (2011).
[17] P. G. De Gennes, J. Fluid Mech. **136**, 189 (1983).
[18] S. Godefroy, J.-P. Korb, M. Fleury, and R. Bryant, Phys. Rev. E **64**, 021605 (2001).
[19] P. L. J. Zitha, G. Chauveteau, and L. Léger, J. Colloid Interface Sci. **234**, 269 (2001).
[20] D. Tiab and E. Donaldson, *Petrophysics: Theory and Practice of Measuring Reservoir Rock and Fluid Properties* (Elsevier, Amsterdam, 2012).

[21] U. M. Scheven, J. G. Seland, and D. G. Cory, Magn. Reson. Imaging **23**, 363 (2005).
[22] P. M. Singer, G. Leu, E. J. Fordham, and P. N. Sen, J. Magn. Reson. **183**, 167 (2006).
[23] L. Lebon, J. Leblond, and J. P. Hulin, Phys. Fluids **9**, 481 (1997).
[24] L. Lebon, L. Oger, J. Leblond, J. P. Hulin, N. S. Martys, and L. M. Schwartz, Phys. Fluids **8**, 293 (1996).
[25] P. P. Mitra, P. N. Sen, L. M. Schwartz, and P. LeDoussal, Phys. Rev. Lett. **68**, 3555 (1992).
[26] U. M. Scheven, D. Verganelakis, R. Harris, M. L. Johns, and L. F. Gladden, Phys. Fluids **17**, 117107 (2005).
[27] R. Lenormand, C. Zarcone, and A. Sarr, J. Fluid Mech. **135**, 337 (1983).
[28] D. G. Avraam and A. C. Payatakes, J. Fluid Mech. **293**, 207 (1995).
[29] K. Tallakstad, G. Løvoll, H. Knudsen, T. Ramstad, E. Flekkøy, and K. Måløy, Phys. Rev. E **80**, 036308 (2009).
[30] J. D. Seymour and P. T. Callaghan, AIChE J. **43**, 2096 (1997).